ELSEVIER

Physica D 96 (1996) 1–8

PHYSICA D

Self-diffusion and relative diffusion in defect turbulence

Greg Huber*, Elsebeth Schröder, Preben Alstrøm

Center for Chaos and Turbulence Studies, Niels Bohr Institute, Blegdamsvej 17, DK-2100 Copenhagen Ø, Denmark

Abstract

We consider the motion of particles and scalar flow in the defect-turbulent regime of the complex Ginzburg–Landau field. We find that the particle motion is diffusion-like at large time scales, whereas the motion is dominated by trapping of particles by defects of the field at short time scales. Consequently the diffusion constant is constrained. For relative motion of two paricles we find that at a relative distance s the distribution of $\mathrm{d}s^2/\mathrm{d}t$ is exponential rather than Gaussian as would be the case for Brownian motion.

Particles are kicked around in a turbulent flow like helium balloons in a hurricane [1]. Their complicated and unpredictable individual and relative motion differ from the Brownian ideal in important ways and present a host of outstanding problems [1–5]. Likewise, the related issue of a turbulently advected passive scalar presents its own analytical difficulties [6–8]. The class of turbulence studied here, defect turbulence, occurs in spatially extended systems near the threshold of a Hopf bifurcation [9,10], which is described in terms of the complex Ginzburg–Landau equation. In two dimensions, defect turbulence is characterized by the motion, creation and annihilation of point defects (vortices). For instance, the two-dimensional complex Ginzburg–Landau equation models the dynamics of oscillatory chemical systems, e.g. the Belousov–Zhabotinsky reaction, and chemical turbulence. In this paper we study the dynamics using passive particles and passive scalars.

* Corresponding author. Present address: The James Franck Institute, University of Chicagco, 5640 S. Ellis Avenue, Chicagco, IL 60637, USA.

We have studied the motion of particles in response to a background field of defect turbulence. We use the complex Ginzburg–Landau equation,

$$\partial_t A(\mathbf{x},t) = A(\mathbf{x},t) - (1+\mathrm{i}\alpha)|A(\mathbf{x},t)|^2 A(\mathbf{x},t) + (1+\mathrm{i}\beta)\nabla^2 A(\mathbf{x},t), \tag{1}$$

for the dynamics of the underlying (complex) amplitude field $A(\mathbf{x},t)$. Here α and β are real numbers, and we take $A = Re^{\mathrm{i}\phi}$. Of crucial importance are the defects of the phase field, i.e. the singularities of $\phi(\mathbf{x},t)$, where the modulus is identically zero: $R(\mathbf{x},t) = 0$. Depending on the values of α and β (Fig. 1), the vortices either appear in a frozen state, where spiral waves in the phase $\phi(\mathbf{x},t)$ wind around fixed vortex cores (Fig. 2(a)), or in a turbulent state where the vortices move rapidly and are annihilated and created in vortex–antivortex pairs [10–13]. The vortices are characterized by their vorticity. The phase gradient points towards the vortex core, except in the area close to the core. There, the gradient lines spiral around the core counterclockwise for vortices of positive vorticity, and clockwise for negative vorticity, Fig. 2(b).

PII S0167-2789(96)00009-7

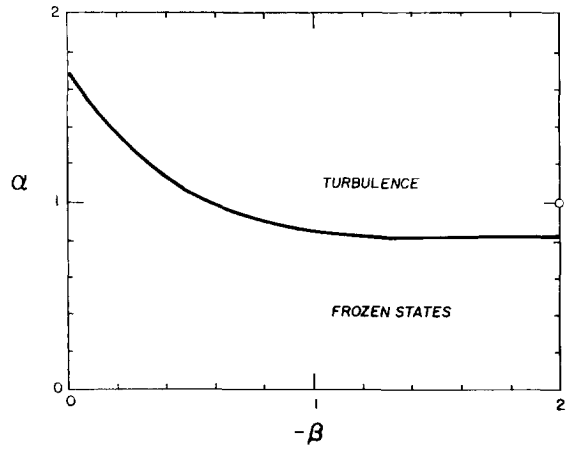

Fig. 1. Phase diagram indicating frozen and turbulent state. The open circle indicates the values used in the simulations ($\alpha = 1$, $\beta = -2$).

The particle is given a velocity

$$\mathbf{v} = \frac{\mathrm{d}\mathbf{r}}{\mathrm{d}t} = \Gamma \nabla \phi(\mathbf{r}, t), \tag{2}$$

where $\mathbf{r}(t)$ is the particle position, and the coefficient Γ is treated as an adjustable parameter (which can be positive or negative). The particle has no inertia in this scheme, the equation of motion being purely dissipative. We are interested in the trajectory and the statistics of particle motion when the underlying field is turbulent. However, for the purposes of illustration, we first consider the particle in the frozen state, where the influence of the defects is clearly discerned and understood.

Eqs. (1) and (2) were discretized using the coupled-map approximation discussed in [11]. We used a 128×128 lattice with periodic boundary conditions, and random initial conditions (A is random within the unit circle). In all cases, we let the system achieve a steady-state vortex density before recording data. The phase gradient at the (off-lattice) particle position $\mathbf{r}$ in Eq. (2) was interpolated from four first-order phase gradients at the four nearest lattice sites.

The motion of the particle in the field of one or a few vortices is the basis by which we understand the more complicated particle motions in the turbulent case. It follows from the choice of the equation of motion (2) that the particle is attracted to the vortices when Γ is positive, and repelled by them when Γ is negative. In the frozen vortex state, the particle will either spiral into a vortex and be trapped, see below, or it will follow the domain walls separating the spiral

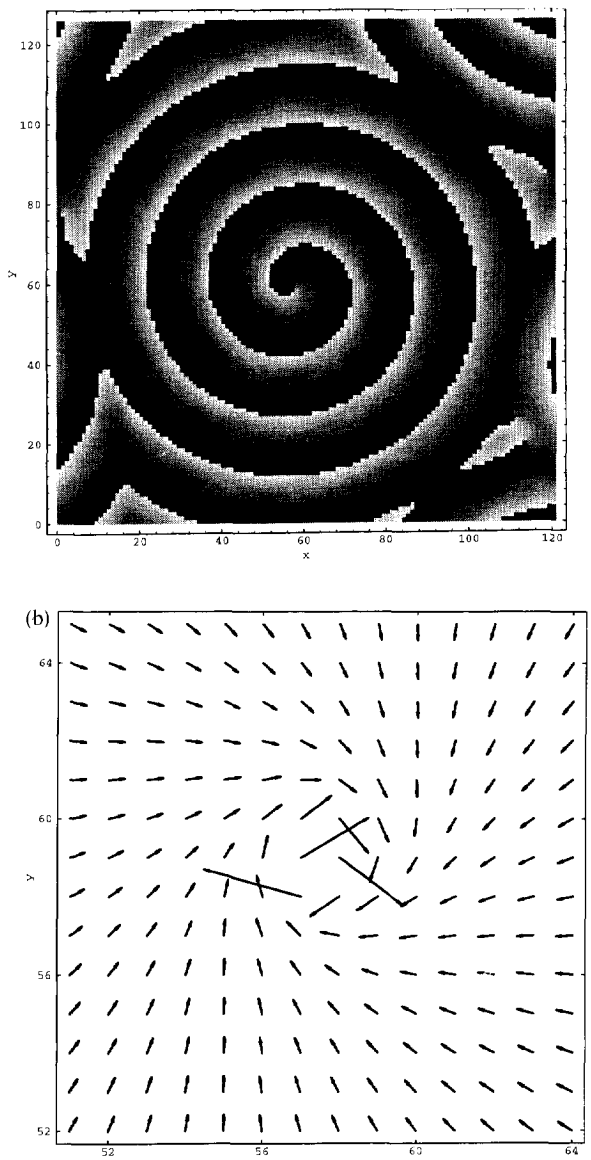

Fig. 2. (a) Phase $\phi(\mathbf{r})$ in a part of a 256×256 system in the frozen state ($\alpha = 0.5$, $\beta = -2$). Black is close to $-\pi$ from above, white is close to π from below. This vortex has negative vorticity ($m = -1$). (b) Phasegradient $\nabla\phi$ in the region around the core of the (same) vortex.

waves until it gets stuck at a junction of three domain walls. In our numerical simulations on a lattice, the spiraling motion into a vortex is eventually replaced by a circulating motion around the vortex core. The phase gradient diverges in the center of the vortex, so in the continuum, the particle velocity keeps increasing. This (unphysical) divergence can be removed by multiplying the right-hand side of Eq. (2) by $|A|$ or $|A|^2$.

In the turbulent regime, and for Γ positive, the particle is still attracted to the vortices and tries to move with them. The lifetime of a vortex in the turbulent field is finite, however, so the particle will eventually be abandoned and must then find and stick to another vortex. The amount of time spent by the particle near a vortex increases with the absolute value of Γ, since increasing $|\Gamma|$ means increasing the velocity of the particle, thereby enabling it to follow the motion of the vortex for a longer period of time. When Γ is sufficiently large, the particle is trapped by the vortex until the vortex undergoes annihilation.

At small time scales we can approximate the phase field $\phi(\mathbf{r}, t)$ in the turbulent state close to the core of a vortex by the phase field of the frozen vortex state. The phase field is described by a fixed core (one-armed) spiral, in polar coordinates [14]

$$\phi(r, \theta, t) = -\omega t + m\theta + \psi(r), \tag{3}$$

where m is the vorticity (± 1 for one-armed spirals), $\omega = \beta k_\infty^2 + \alpha(1 - k_\infty^2)$ is the frequency of rotation and k_∞ is the asymptotic wave number of the spiral, $k_\infty^2 < 1$. The wave number k_∞ depends on the parameters α and β, and has not been found analytically. Close to the core the radial dependence of the phase field may be approximated by

$$\psi(r) = d_2 r^2 + d_4 r^4 + \cdots \tag{4}$$

By inserting this into a polar coordinates version of (1) one finds the coefficients, the first of which is

$$d_2 = \frac{-\omega + \beta}{4(|m| + 1)(1 + \beta^2)} = \frac{(\beta - \alpha)(1 - k_\infty^2)}{4(|m| + 1)(1 + \beta^2)}. \tag{5}$$

The velocity of the particle is, in polar coordinates $[\nabla = \hat{\mathbf{r}}\partial_r + \hat{\boldsymbol{\theta}}\frac{1}{r}\partial_\theta]$,

$$\mathbf{v} = \Gamma(\hat{\mathbf{r}}\partial_r + \hat{\boldsymbol{\theta}}\frac{1}{r}\partial_\theta)\phi = \hat{\mathbf{r}}\Gamma\partial_r\psi(r) + \hat{\boldsymbol{\theta}}\frac{m\Gamma}{r}, \tag{6}$$

which to lowest order in r can be integrated to give

$$r(t) = r_0 e^{2\Gamma d_2 t},$$

$$\theta(t) = \theta_0 - \frac{m}{4r_0^2 d_2}(e^{-4\Gamma d_2 t} - 1). \tag{7}$$

The coefficient d_2 contains the asymptotic wavelength k_∞ and therefore has to be found numerically. In the frozen state k_∞ may be obtained directly from the spirals around the vortices, such as in Fig. 2(a). In the turbulent state this is not possible because the vortices move around too fast for spirals to form. Instead, to estimate d_2 the particle motion may be compared to Eq. (7).

Figs. 3(a) and (b) show the traces of a particle moving with $\Gamma = 1$ and $\Gamma = 10$. We used $\alpha = 1$ and $\beta = -2$ (open circle in Fig. 1). Complete trapping is observed for $\Gamma = 10$. Fitting the trajectories of the particles in the simulations to (the start of) the spiral motion we find $d_2 = -0.03 \pm 0.02$. d_2 is very sensitive to changes in the values of the initial radius r_0 and the time for the first half period ($\theta = \theta_0 + \pi$), so our result should merely be taken as an indication of the spiraling motion of the particles when trapped at a vortex. It may be compared to the value of d_2 obtained in the frozen state, e.g. for $\alpha = 0.5$ and $\beta = -2$, by two different methods: A fit of a third-order polynomial in r to the phase $\phi(\mathbf{r})$ for a fixed angle θ and time t gives $d_2 = -0.09 \pm 0.05$, and vanishing coefficients for the first- and third-order terms as expected from Eq. (4). d_2 may also be obtained by measuring the asymptotic wavelength from Fig. 2(a), $\lambda_\infty = 2\pi/k_\infty = 15 \pm 1$, Eq. (5) then gives $d_2 = -0.052 \pm 0.002$. We find that the value of d_2 in the turbulent state is of the same order of magnitude as d_2 in the frozen state, and possibly slightly smaller. A smaller d_2 would give a larger k_∞ (tighter wound spirals) if spirals were able to exist in the turbulent state. For negative Γ, the particle is repelled by the vortices, so no trapping is observed (Fig. 3(c)).

The intriguing combination of vortex pinning and the motion between the vortices is even more emphasized when plotting the time variation of the "energy"

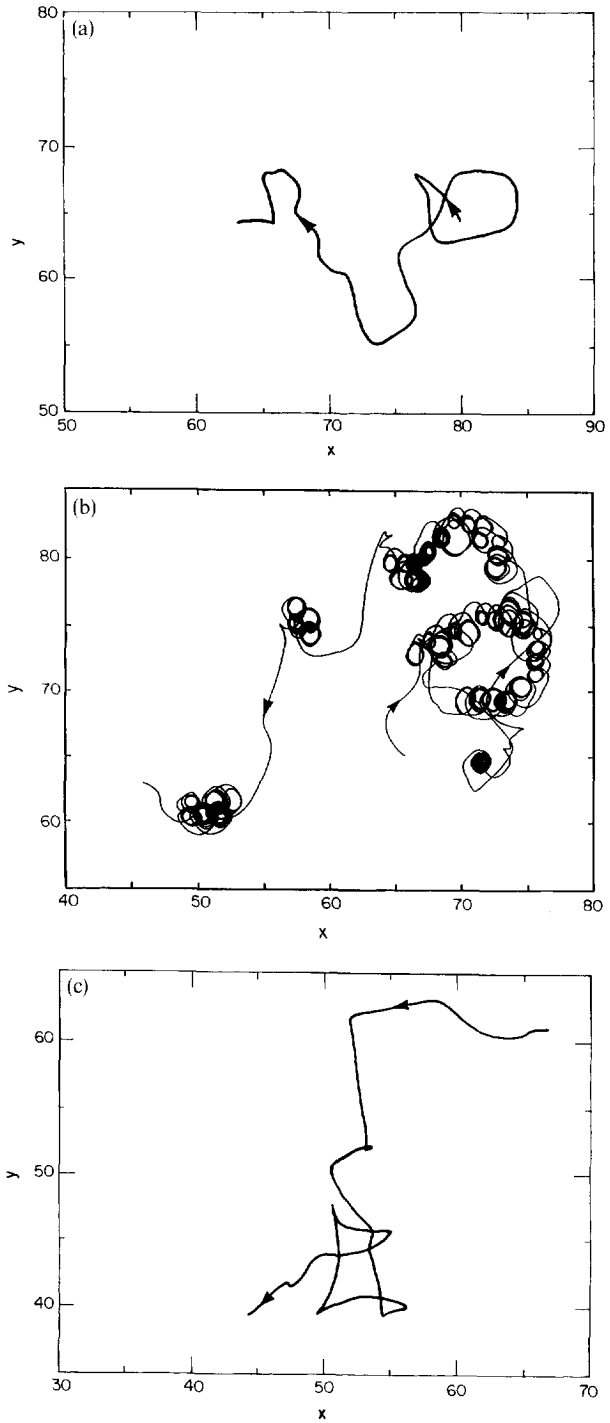

Fig. 3. Particle traces in the turbulent state, system size 128 × 128, for the parameter values (a) $\Gamma = 1$, (b) $\Gamma = 10$, (c) $\Gamma = -1$.

$\epsilon \equiv \mathbf{v}^2$. This is shown in Fig. 4, revealing a very intermittent behavior. As seen, ϵ is large while the particle is trapped by a vortex, indicating that the phase gradients close to the vortices are large. When the particle moves between vortices, ϵ decreases drastically to a small value.

To study self-diffusion, we consider the mean square displacement $\langle \Delta r^2 \rangle$ of the particle as a function of the time interval Δt. In Fig. 5(a) $\langle \Delta r^2 \rangle$ is plotted versus Δt on double-logarithmic scale for $\Gamma = 1, 10, 100$. The inset shows a longer run for $\Gamma = -1.2$. At low Δt we find that the motion is ballistic, $\langle \Delta r^2 \rangle \propto (\Delta t)^2$, while at large time intervals the motion seems to approach normal diffusion, $\langle \Delta r^2 \rangle = D \Delta t$ where D is the self-diffusion constant.

Fig. 5(b) shows the diffusion constant D obtained as a function of Γ. When $|\Gamma| << 1$, we find that $D \propto \Gamma^2$. The appropriate physical picture in this case is that of a particle being kicked about by an underlying random vector field. In this picture, a squared displacement of $\langle \Delta r^2 \rangle$ will be proportional to Δt, with a prefactor proportional to $\Gamma^2 \langle |\nabla \phi|^2 \rangle$. As the value of Γ increases, the vortex trapping of particles becomes more efficient, and a hump develops in the mean square displacement curve (Fig. 5(a)). Only well beyond the time the particle is trapped by a vortex, the diffusion law is recovered. The trapping effect indicates that the self-diffusion constant eventually is limited to that of the vortex diffusion. Accordingly, at large Γ we find that the velocity of the particle is large enough to follow any motion of the vortices. Thus, it is solely the underlying field dynamics that determines the dynamics of the particle. In this case ($|\Gamma| >> 1$), D is independent of Γ, as seen in Fig. 5(b).

The motion of one particle relative to another in a turbulent field is called Richardson diffusion. If $\mathbf{s} \equiv \mathbf{r}_2 - \mathbf{r}_1$ denotes the position of particle 2 relative to particle 1, an important question in the field of turbulence is the dependence of $D(s) = \langle \mathrm{d}s^2/\mathrm{d}t \rangle$ on the distance $s = |\mathbf{s}|$. If $D(s)$ is constant, the relative motion is diffusion-like. In general, two advected particles will probe velocity correlations on scales of order their separation.

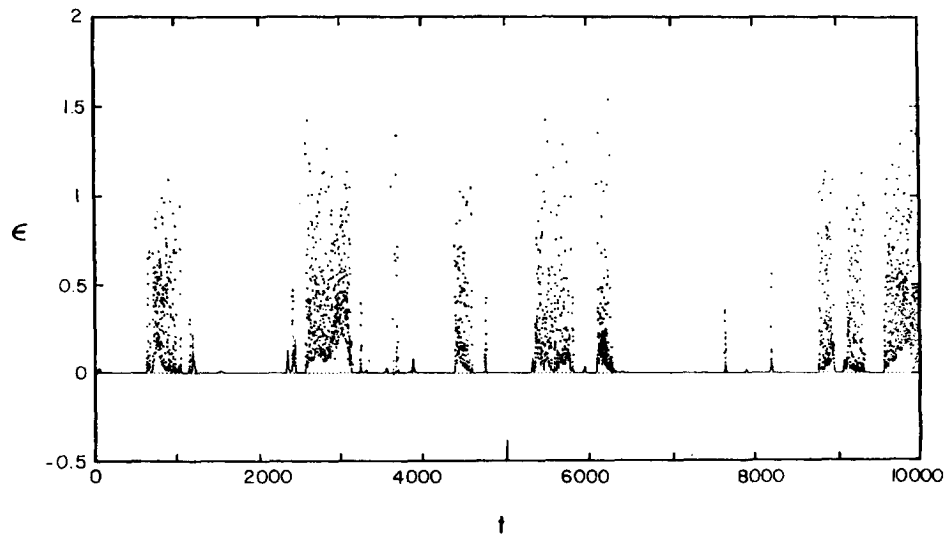

Fig. 4. Energy $\epsilon = \mathbf{v}^2(t)$.

In order to determine $D(s)$ we follow two routes: One is the Eulerian, where two lattice points at distance s apart are selected, and at any given time two particles are launched and followed for one time step to determine $\mathrm{d}\mathbf{s}^2/\mathrm{d}t$. The other route is the Lagrangian, where two particles are launched and followed in time, sampling $\mathrm{d}\mathbf{s}^2/\mathrm{d}t$ as a function of t. From the first $D(s)$ is obtained directly, averaging over time. From the second approach, the values of $\mathrm{d}\mathbf{s}^2/\mathrm{d}t$ for various values of s are collected from many traces of particle pairs, or from very long traces, where the pair of particles are at distance s apart many times.

Fig. 6(a) shows a semi-logarithmic plot of the distribution $P(D)$ for $s=75$ and $s=200$ obtained from the Lagrangian approach. The mean value is very small compared to the width of the distribution, so no conclusive results are obtained for the s dependence of $D(s)$. This is also the case for the Eulerian approach. However, $P(D)$ is clearly not Gaussian, as is found for Brownian motion. Rather the distributions fall off exponentially. We find that the width increases linearly with s for both the Lagrangian and the Eulerian approach (Fig. 6(b)).

We find when launching many particles that these in the course of time merge (Merging has also been observed for the one-dimensional Kuramoto–Sivashinskii equation [15]). To illustrate the effective particle field, we comment on using a passive scalar field with Eq. (1):

$$\partial_t \Theta + \nabla \cdot (\mathbf{v}\Theta) = \mathcal{K}\nabla^2\Theta. \tag{8}$$

Fig. 7 shows the particle concentration in grey code. We have used a non-zero diffusivity $\mathcal{K} = 1$, and the velocity $\mathbf{v} = \nabla\phi$. It is clear that the concentration is not homogeneous. Rather, spikes are observed in the particle concentration corresponding to the location of the vortices. For the velocity $\mathbf{v} = -\nabla\phi$ the concentration is at its maximum at boundaries between the domains of the vortices.

In conclusion, we have analyzed particle motion in the two-dimensional Ginzburg-Landau field. On long time scales the motion seems to be diffusion-like. However, the trajectories are heavily constrained by trapping at vortices, which puts an upper limit on the diffusion constant. The trapping gives rise to an intermittent behavior of the energy $\propto \mathbf{v}^2$. We have also considered relative diffusion, and we find that the distribution of $\mathrm{d}s^2/\mathrm{d}t$ for a given s is exponential rather than Gaussian as is the case for Brownian motion.

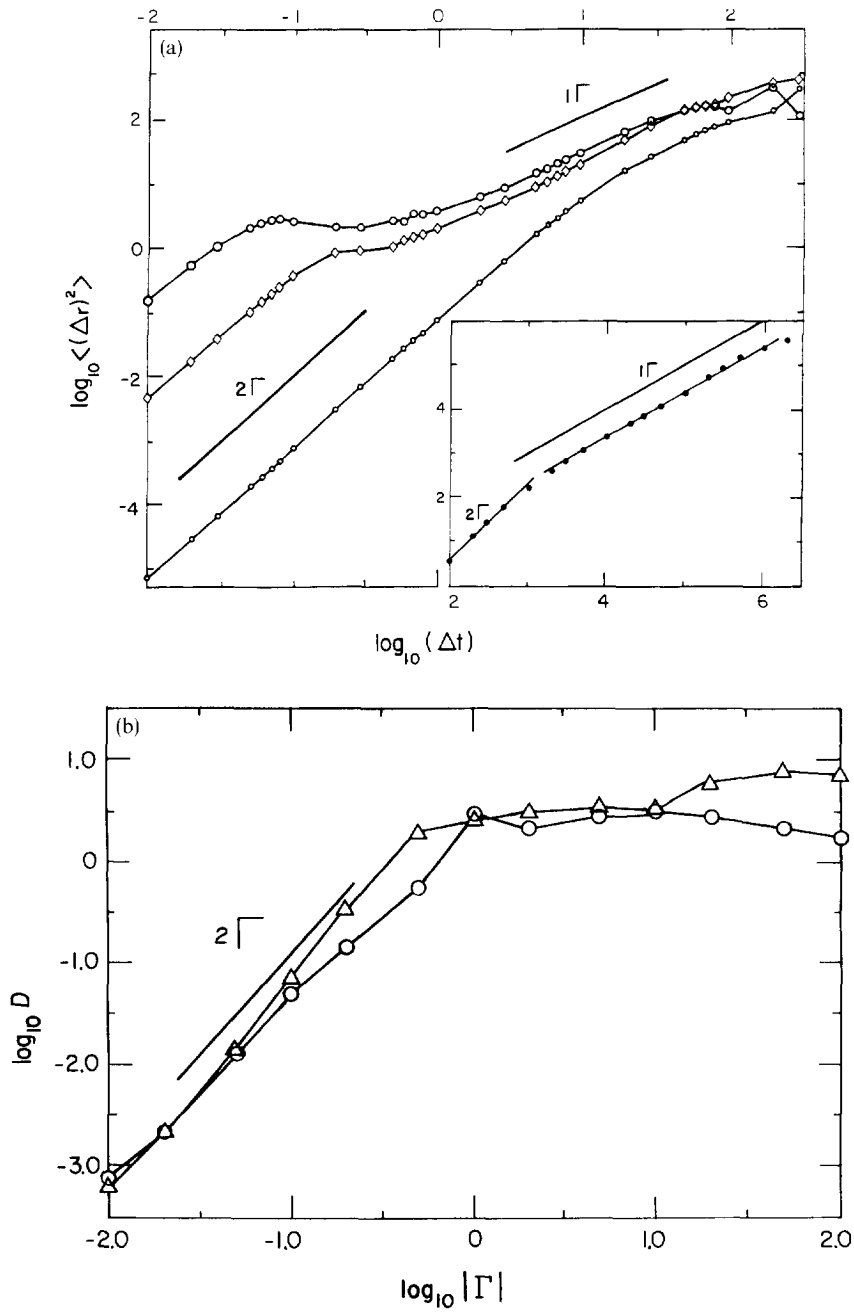

Fig. 5. (a) The mean square distance $\langle \Delta r^2 \rangle$ versus t for $\Gamma = 1$ (small circles), $\Gamma = 10$ (diamonds), $\Gamma = 100$ (big circles). System size 128×128. Inset: $\langle \Delta r^2 \rangle$ versus t for $\Gamma = -1.2$. (b) The self-diffusion coefficient D as a function of the parameter $|\Gamma|$, double-logarithmic scale. $\Gamma < 0$: triangles, $\Gamma > 0$: circles.

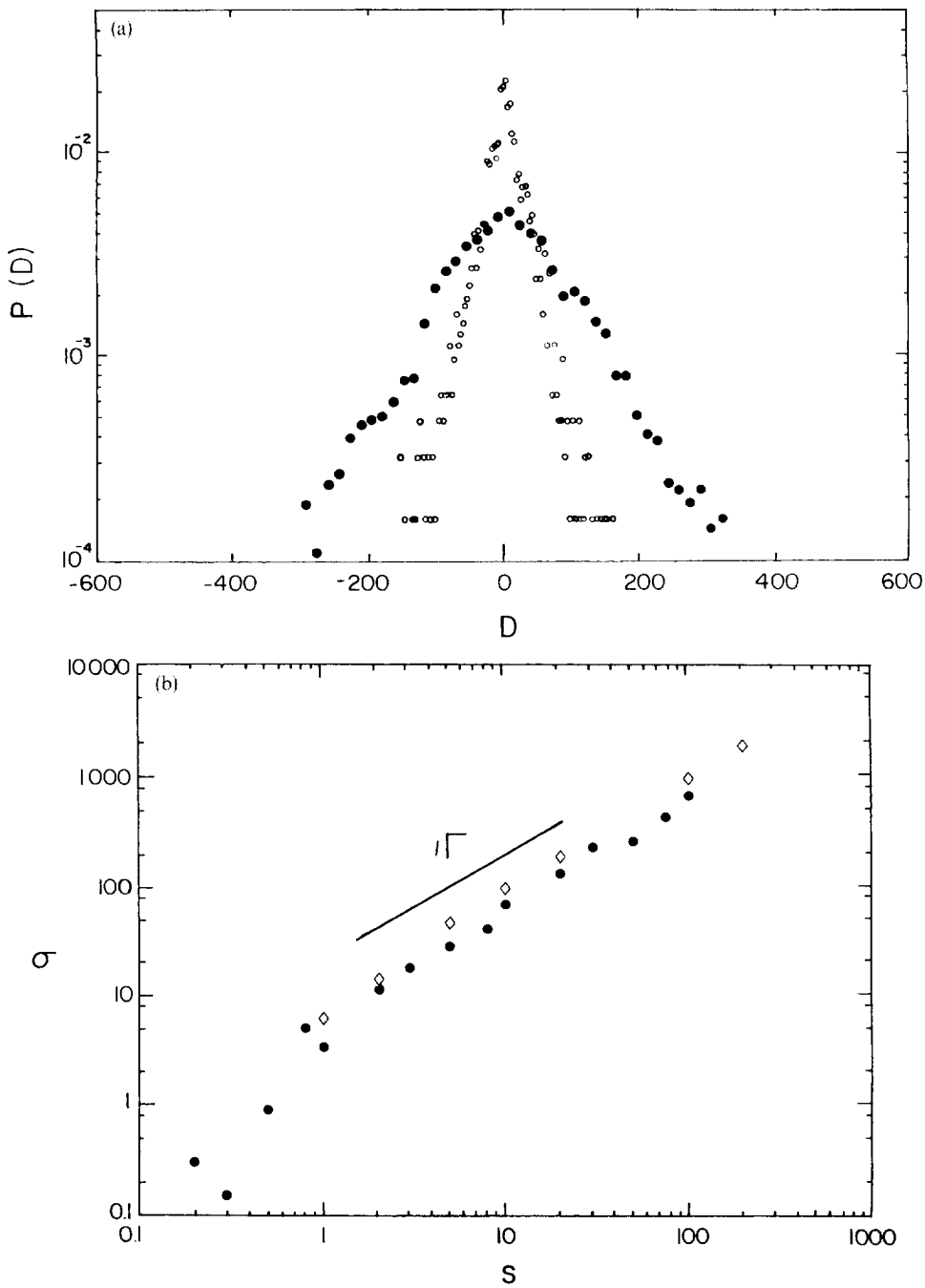

Fig. 6. (a) Distribution $P(D)$ for the Lagrangian approach. Distances between particles are $s = 75$ (open circles) and $s = 200$ (black circles) for the parameter $\Gamma = 1$. (b) Width $\sigma(s)$ of the distribution functions for the Eulerian (diamonds) and the Lagrangian approach (black circles). $\Gamma = 10$.

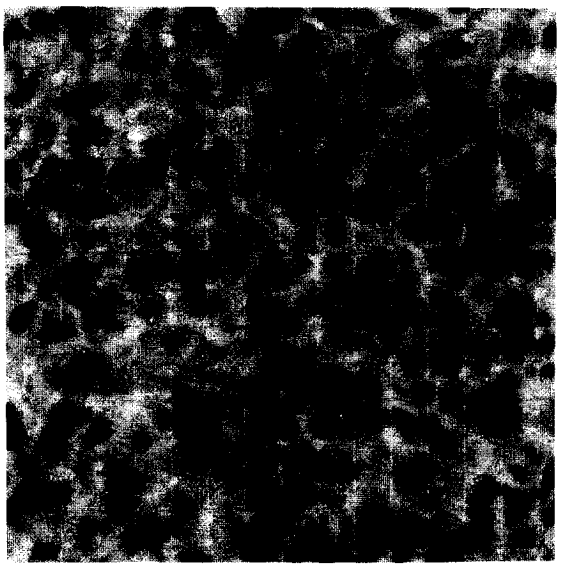

Fig. 7. Particle concentration in grey code for the case of a passive scalar. Black is maximum. The velocity field is given by $\mathbf{v} = \nabla\phi$, the system size is 256×256 and the diffusivity is $\mathcal{K} = 1$.

Acknowledgements

This work was supported by the Novo-Nordisk Foundation, the Danish Natural Science Research Council, and the Danish Research Academy.

References

[1] L.F. Richardson, Proc. Roy. Soc. London Ser. A 110 (1926) 709.
[2] F. Gifford Jr., J. Meteorology 14 (1957) 410.
[3] H.G.E. Hentschel and I. Procaccia, Phys. Rev. A 28 (1983) 417.
[4] R. Ramshankar, D. Berlin and J.P. Gollub, Phys. Fluids A 2 (1990) 1955.
[5] P. Alstrøm, J.S. Andersen, W.I. Goldburg and M.T. Levinsen, Chaos, Solitons and Fractals 5 (1995) 1455.
[6] R. Ramshankar and J.P. Gollub, Phys. Fluids A 3 (1991) 1344.
[7] P. Constantin, I. Procaccia and K.R. Sreenivasan, Phys. Rev. Lett. 67 (1991) 1739.
[8] I. Procaccia and P. Constantin, Europhys. Lett. 22 (1993) 689.
[9] Y. Kuramoto, Chemical Oscillations, Waves, and Turbulence (Springer, Berlin, 1984).
[10] P. Coullet, L. Gil and J. Lega, Phys. Rev. Lett. 62 (1989) 1619; L. Gil, J. Lega and J.L. Meunier, Phys. Rev. A 41 (1990) 1138.
[11] T. Bohr, A.W. Pedersen, M.H. Jensen and D.A. Rand, in: New Trends in Nonlinear Dynamics and Pattern Forming Phenomena: The Geometry of Nonequilibrium, eds., P. Coullet and P. Huerre (Plenum Press, New York, 1989); T. Bohr, A.W. Pedersen and M.H. Jensen, Phys. Rev. A 42 (1990) 3626; X.-G. Wu and R. Kapral, J. Chem. Phys. 94 (1991) 1411.
[12] I.S. Aranson, L. Aranson, L. Kramer and A. Weber, Phys. Rev. A 46 (1992) R2992.
[13] G. Huber, P. Alstrøm and T. Bohr, Phys. Rev. Lett. 69 (1992) 2480.
[14] P.S. Hagan, SIAM J. Appl. Math. 42 (1982) 762.
[15] T. Bohr and A. Pikovsky, Phys. Rev. Lett. 70 (1993) 2892.